Cryogenic Charge Transport in Oxidized Purple Bacterial Light-Harvesting 1 Complexes

Nagarajan Srivatsan

Avery Research Center, 2900 Bradley Street, Pasadena, California 91107

Dmitri Kolbasov and Nina Ponomarenko

Department of Chemistry, University of Chicago, 5735 South Ellis Avenue, Chicago, Illinois 60637

Stefan Weber

Institute of Experimental Physics, Free University Berlin, Arnimallee 14, 14195 Berlin, Germany

Agnes E. Ostafin

Department of Chemical Engineering, University of Notre Dame, 182 Fitzpatrick, Notre Dame, Indiana 46556

James R. Norris, Jr.*

Department of Chemistry and Institute of Biodynamics, University of Chicago, 5735 South Ellis Avenue, Chicago, Illinois 60637

Received: December 16, 2002; In Final Form: April 22, 2003

We report on the analysis of the inter-bacteriochlorophyll *a* (BChl*a*) charge-transport process that occurs in oxidized purple bacterial light-harvesting 1 (LH1) complexes. Experimentally, charge migration within oxidized LH1 is monitored by following the temperature-dependent changes of the BChl$a^{\bullet+}$ electron paramagnetic resonance (EPR) line-shape characteristics. At 6 K, a Gaussian-shaped spectrum with a 1.3-mT width is detected. These characteristics indicate that at extremely low temperatures charge transport is substantially slowed so that the unpaired electron is localized on one or two BChl*a*s. At higher temperatures, the spectra exhibit non-Gaussian line shapes and decreased line widths. These characteristics are engendered by charge migration. We have analyzed the temperature dependence of the transport process through EPR spectral simulations. The simulations incorporated a nonadiabatic model for electron transfer. The temperature dependence could be adequately described on the basis of an electron-transfer model that accounts for the effects of slow medium relaxation, whereas a satisfactory description could not be obtained on the basis of conventional multimode models for transport. The results of our analysis are consistent with the notion that the protein functions as the primary solvent for the redox centers and are in accord with the view that the protein behaves as a frozen glass, even at room temperature, with respect to the low-frequency vibrational motions coupled to electron transfer.

I. Introduction

A significant amount of contemporary research is dedicated to elucidating the energetic and electronic factors that impact biological electron transfer. In this regard, synthetic and semisynthetic model compounds and natural systems have been extensively investigated, leading to a fairly detailed understanding of the free-energy dependence and distance dependence of the electron-transfer rates.[1,38] Recent theoretical and experimental developments have brought into focus an important facet of electron transfer in proteins concerning the glassy environment presented by the matrix to the redox cofactors.[2,3] The investigations indicate that slow medium relaxation in glassy environments can lead to situations where the full reorganization energy becomes unavailable and suggest that such effects can profoundly affect the temperature dependence of the electron-transfer rates. We have previously reported on the charge-transport process in oxidized light-harvesting 1 (LH1) complexes from *Rhodobacter* (*Rb.*) *sphaeroides*[4] and *Blastochloris* (*B.*) *viridis*.[22] In this work, we analyze the temperature dependence of the rates using a model that describes electron transfer in glassy media and compare the results to those obtained on the basis of standard models for nonadiabatic transport. The analysis indicates that medium relaxation effects significantly impact charge transport in oxidized LH1. Our results, together with conclusions of other recent investigations,[3,5] suggest that slow dynamics of the protein/solvent system may be a characteristic that generally impinges upon the energetics and hence the temperature dependence of electron-transfer processes in biological systems.

The structure of LH1 has been reasonably well characterized through biochemical and electron microscopy investigations.[6−11] The integral-membrane complexes are oligomers of the light-harvesting pigments, which are bacteriochlorophylls and carotenoids, and low molecular weight hydrophobic polypeptides.[6] In bacteriochlorophyll *a* (BChl*a*) containing species such as *Rb. sphaeroides*, the LH1 basic unit consists of two similar membrane spanning peptides, α and β, that bind one BChl*a* each. Electron micrographs of LH1 complexes in numerous instances have indicated that the $\alpha\beta$ units form circular oligomers.[7−10] The 0.85-nm-resolution projection map determined for LH1 from *Rhodospirillum* (*Rs.*) *rubrum*, for instance, shows quite clearly a ring composed of 16 $\alpha\beta$ units.[7] Rings of similar dimensions are also detected for complexes from *Rb.*

* Corresponding author. E-mail: j-norris@uchicago.edu. Phone: +1 (773) 702-7864. Fax: +1 (773) 702-0805.

10.1021/jp027736y CCC: $25.00
Published on Web 06/28/2003

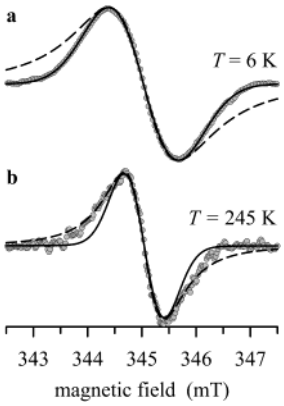

Figure 1. Temperature dependence of X-band (9.0−9.5 GHz) B880$^{\bullet+}$ EPR spectra.[4,15] The radical cations were generated by the oxidation of detergent-isolated LH1 ($A_{882\ nm} \approx 2.1$) with an 8-μM final concentration of potassium ferricyanide. The symbols denote the experimental spectra, and the solid and dashed lines represent Gaussian and Lorentzian curves, respectively, that were calculated with the peak-to-peak widths of the experimental spectra. The 6 K spectrum (panel a) is characterized by a Gaussian shape and a 1.3-mT width. The B880$^{\bullet+}$ line shape becomes non-Gaussian, and the line width decreases when the temperature is increased above 6 K. These characteristics are clearly discerned, for instance, in the 245 K spectrum (panel b). The B880$^{\bullet+}$ line shape at 245 K is seen to be intermediate between the Gaussian and Lorentzian curves, and the width is narrowed to 0.73 mT. The temperature-dependent changes in the B880$^{\bullet+}$ spectral characteristics are due to the thermally activated transport of electrons/holes within the B880 oligomers. The apparent magnetic field shifts in the spectra are due to small shifts of the resonance frequency of the microwave resonator upon changing the sample temperature.

sphaeroides.[9] The LH1 BChl*a*s are also designated as B880 because of the characteristic 880-nm absorption exhibited by the pigments. The B880s are thought to form an overlapping circular array sandwiched between concentric rings formed by the α and β peptides.[12] This notion is based on the extensive structural and optical spectroscopic analogies exhibited by LH1 to LH2 complexes, the crystal structures of which reveal such an architecture.[13,14]

Our previous investigations demonstrated that mobile holes are generated upon oxidation of the B880s to the corresponding radical cations (B880$^{\bullet+}$).[4,15] The itinerant nature of the holes is revealed by the observed temperature-dependent changes of the electron paramagnetic resonance (EPR) line-shape characteristics. The EPR experiments were conducted at X-band frequencies (9.0−9.5 GHz) on B880$^{\bullet+}$ elicited with potassium ferricyanide. At 6 K, and for very mildly oxidized samples, a Gaussian B880$^{\bullet+}$ spectrum with a 1.3-mT width is detected (Figure 1a). Such Gaussian spectra are typical for magnetically dilute BChl$^{\bullet+}$ species at X-band frequencies.[16] The shape is a consequence of inhomogeneous broadening of the spectrum, where the main broadening contribution accrues from electron−nuclear hyperfine interactions. The Gaussian shape also directly indicates the absence of motion on the X-band EPR time scale. Upon increasing the temperature, a Gaussian-to-non-Gaussian transition of the spectral shape is observed concomitantly with a decrease in the line width (Figure 1b). The shape changes and width decreases, which are due to the modulation of the hyperfine interactions, reveal motion on the X-band time scale. The inter-B880 charge-migration process is conveniently monitored by following the changes in the line width with temperature (Figure 2). The large systematic width decrease observed upon warming from 6 to 255 K shows that the rates progressively increase with increasing temperature.

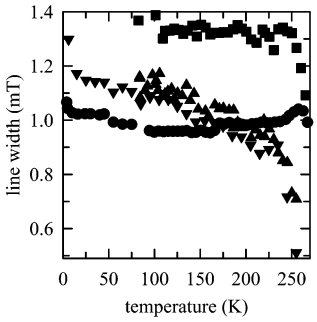

Figure 2. EPR line width versus temperature profiles of B880$^{\bullet+}$.[4,15] The radical cations were elicited by the oxidation of detergent-isolated LH1 ($A_{882\ nm} \approx 2.1$) with (▲) 7 and (▼) 8 μM final concentrations of potassium ferricyanide. The line width versus temperature profiles of P865$^{\bullet+}$ (●) and B820$^{\bullet+}$ (■) are also shown for comparison. These radical cations were also generated with potassium ferricyanide. P865$^{\bullet+}$ consists of a strongly coupled dimer of bacteriochlorophyll *a* (BChl*a*) molecules, and it is the radical cation of the primary electron donor of photosynthetic reaction centers. Various electron paramagnetic resonance experiments have indicated that P865$^{\bullet+}$ is best considered to be a strongly delocalized supermolecular radical cation.[16,35] Overall, the P865$^{\bullet+}$ EPR width (●) does not vary much in the 6−295 K range, and the spectral shape remains approximately Gaussian.[36] The decrease of about 0.7 mT detected between 6 and 100 K is due to the activated rotations of methyl groups located on rings I and III of the macrocycles.[26] B820$^{\bullet+}$ is the radical cation of the $\alpha\beta$(BChla_2) subunit that is isolated following detergent titration of carotenoid-deficient LH1 (B880) complexes. The B820$^{\bullet+}$ EPR width (■) shows a precipitous decrease from 1.33 mT starting at about 245−250 K due to a rapid increase of inter-BChl*a* charge-transport rates.[15] The B880$^{\bullet+}$ EPR width (▲, ▼) exhibits a substantial variation in the 6−255 K temperature range due to activated charge transport within the B880 oligomers.[4] Similar to B820$^{\bullet+}$, the B880$^{\bullet+}$ width exhibits a precipitous change at about 245 K due to rapid rate variations that occur at this temperature.

The inter-B880 charge-transport process is indirectly detected through the influence that it has on the B880$^{\bullet+}$ EPR spectral shape and width. Consequently, details regarding the process must be extracted through a comparison of simulations, based on an appropriate EPR model, to experimental data. In this work, we have conducted simulations with an EPR model that incorporated Hoffman and Ratner's description of electron transfer in glassy media and, separately, Hopfield's model and Tang's model for nonadiabatic transport.[2,17,18] This work is focused on oxidized detergent-isolated LH1 complexes from *Rb. sphaeroides*. It is nevertheless expected that the broader conclusions of the analysis will apply to oxidized LH1 complexes in general because essentially identical narrow room-temperature EPR spectra with widths of about 0.4 mT are detected for oxidized detergent-isolated and membrane-bound LH1 complexes from various types of photosynthetic bacteria including *Rb. sphaeroides*,[4,20] *Rs. rubrum*,[19−21] and *B. viridis*[22] and LH1 complexes from various species exhibit similar compositions and structures.[6] The remainder of the article is organized as follows: the EPR line-narrowing model and electron-transfer models used for the spectral simulations are described in section II, the results of the analysis are reported and discussed in section III, and a summary of the work is given in section IV.

II. Analysis Models

A. EPR Line Narrowing. The EPR line-narrowing model utilized for the present analysis is based on the "random frequency modulation" model of Anderson[23] and Kubo[24] and has been reported by us earlier.[4] Here we outline the general aspects of our approach. It is first assumed that electron−nuclear

hyperfine interactions alone constitute the line-broadening process. This assumption is consistent with the Gaussian shape of the 6-K $B880^{\bullet+}$ spectrum. As mentioned earlier, the Gaussian shape is rather typical for magnetically dilute $BChl^{\bullet+}$ species at X-band frequencies, where the major contribution to the inhomogeneous broadening accrues from electron−nuclear hyperfine interactions.[16] According to the hyperfine interaction mechanism, the transitions contributing to the spectrum are engendered by radical cations with different local magnetic environments. The distribution of magnetic environments is originated by the different nuclear spin configurations on the various molecules in the ensemble. Because the nuclear spin and electron spin relaxation times are rather long, as is directly indicated in the case of $B880^{\bullet+}$ by the Gaussian line shape at 6 K, the spectrum can be taken to represent a static distribution on the time scale of the X-band experiment. The *N*-mers are considered to be groups of *N* molecules chosen from this distribution. The nuclear spin configurations at the various sites occur in a mutually independent manner. For this reason, the probabilities of obtaining the various *N*-mers are $P(\omega_1, \omega_2,..., \omega_N) = P(\omega_1) \times P(\omega_2) \times ... \times P(\omega_N)$, where the ω_i's represent the resonance frequencies or fields of the electron spin at the various sites. The *N*-mers occurring with the aforesaid probabilities are assumed to constitute subensembles, as is standard practice.[25] The observed *N*-mer spectrum is the sum of the spectra of all possible subensembles.

The subensemble spectra are obtained from the Fourier transform of the magnetic moment autocorrelation function, where the autocorrelation function incorporates the effect of frequency or field fluctuations due to motion. The present line-narrowing problem is identical to the well-known case where the resonance frequency or field executes transitions between *N* states. For this system, assuming a Markovian transition process and neglecting saturation effects, Anderson and Kubo have derived the autocorrelation function as[23,24]

$$S(t) = \boldsymbol{\varphi} \exp[(i\boldsymbol{\Omega} + \mathbf{W})t]\phi \qquad t > 0$$
$$S(-t) = S^*(t) \tag{1}$$

where $\boldsymbol{\varphi}$ is a vector with *N* elements (φ_i) that are proportional to the equilibrium occupational probabilities, ϕ is a vector with *N* elements equal to unity, and $\boldsymbol{\Omega}$ is an $N \times N$ diagonal matrix with elements equal to the resonance or field frequency of the spin at the various sites. The $N \times N$ matrix $\mathbf{W}$ contains elements

$$\left.\begin{aligned} w_{ij} &= k_{j\rightarrow i} \\ w_{ii} &= -T_2^{-1} - \sum_{j=1}^{N} w_{ji} \end{aligned}\right\} (i \neq j) \tag{2}$$

where $k_{j\rightarrow i}$ is the spin-motion rate from the *j*th site to the *i*th site and T_2^{-1} is the electron spin transverse relaxation time. The autocorrelation function, $S(t)$, is computed by diagonalizing ($i\boldsymbol{\Omega} + \mathbf{W}$) so that it is expressed as a sum of exponentials. The real part of the Fourier transform of $S(t)$ is the line-shape function, $I(\omega)$, which is represented as

$$I(\omega) \propto -\sum_{i=1}^{N} \frac{\mathrm{Re}(c_i)\,\mathrm{Re}(\lambda_i) + \mathrm{Im}(c_i)[\mathrm{Im}(\lambda_i) - \omega]}{\mathrm{Re}(\lambda_i)^2 + [\mathrm{Im}(\lambda_i) - \omega]^2}$$
$$c_i = \sum_{j=1}^{N} \varphi_j u_{ji} \sum_{k=1}^{N} v_{ik} \tag{3}$$

where Re and Im denote the real and imaginary parts, respectively, of the complex numbers, u_{ji} and v_{ik} are the elements of the matrix of eigenvectors and its inverse, respectively, that diagonalizes ($i\boldsymbol{\Omega} + \mathbf{W}$), and λ_i are the corresponding eigenvalues and the subscripts *i*, *j*, and *k* are integer values.

The *N*-mer spectral simulations were conducted in the field domain according to the following procedure. The subensembles were generated by selecting groups of *N* fields using a Gaussian random number generator. The matrices ($i\boldsymbol{\Omega} + \mathbf{W}$) were formed and computationally diagonalized to obtain vectors containing the eigenvalues and matrices containing the corresponding eigenvector components, following which the inverses of the eigenvector matrices were computed. The subensemble spectra were calculated according to eq 3 and then added to yield the ensemble averaged spectrum ($\bar{I}(\omega)$). The shape of $\bar{I}(\omega)$ converged when about 2×10^6 subensemble spectra were summed. Finally, first-derivative spectra ($\bar{I}'(\omega)$) were calculated by numerically differentiating digitally filtered absorption-mode spectra. Figure 3 illustrates some pertinent characteristics of motionally narrowed spectra for *N*-mers.

B. Electron Transfer. Hoffman and Ratner's description of electron transfer in glassy media is based on Hopfield's model for nonadiabatic processes. In both approaches, transport is considered to be coupled to two modes, $\nu_{(o)}$ and $\nu_{(i)}$, that represent low-frequency outer-sphere and high-frequency inner-sphere motions, respectively.[2,17] In the Hoffman−Ratner model, molecular motions represented by $\nu_{(o)}$ are strongly damped by the glassing of the medium upon decreasing the temperature, but vibrations represented by $\nu_{(i)}$ are unaffected.[2] The free-energy gap and the reorganization energy are assumed to undergo correlated changes with temperature such that their sum remains temperature-independent. The particular assumption is that $\Delta G(T) + \lambda(T) = \Delta G^0 + \lambda_s$, where $\Delta G(T)$ and $\lambda(T)$ are the free-energy gap and reorganization energy, respectively, at a temperature *T*, and ΔG^0 and λ_s are the free-energy gap and reorganization energy, respectively, for the equilibrium electron-transfer reaction. The total equilibrium reorganization energy, λ_s, is the sum of the equilibrium outer (λ_o) and inner (λ_i) sphere contributions. Because only low-frequency motions are assumed to be affected by medium glassing, the temperature dependence of $\lambda(T)$ is attributed to changes in λ_o alone. Incorporating these assumptions for the reaction energetics into Hopfield's two-mode expression, the electron-transfer rate constant was derived as[2]

$$k = \frac{\sqrt{\pi}}{\hbar} \frac{V^2}{\sqrt{B_H}} \exp\left[-\frac{(\Delta G^0 + \lambda_s)^2}{4B_H}\right]$$
$$B_H = k_B T_c^{(o)} \lambda_o(T) \coth\left(\frac{2T_c^{(o)}}{T}\right) + k_B T_c^{(i)} \lambda_i \coth\left(\frac{2T_c^{(i)}}{T}\right) \tag{4}$$
$$\lambda(T) = \lambda_i + \lambda_o(T) = \lambda_i + f(T)\lambda_o$$
$$f(T) = \begin{cases} \exp\left[-\dfrac{B}{T - T_g}\right], & T > T_g \\ 0, & T < T_g \end{cases}$$

where *V* is the electronic coupling matrix element and $T_c^{(o)}$ and $T_c^{(i)}$ are defined in terms of the corresponding vibrational frequencies as $T_c^{(\alpha)} = (h\nu_{(\alpha)}/k_B)$. In the function $f(T)$, which describes medium glassing, T_g is an equilibrium glass-transition temperature below which it is assumed that low-frequency medium motion is frozen and *B* is a pseudoactivation energy for medium motion at $T > T_g$. The reorganization energy $\lambda(T)$ varies from λ_i when the low-frequency motion is halted below

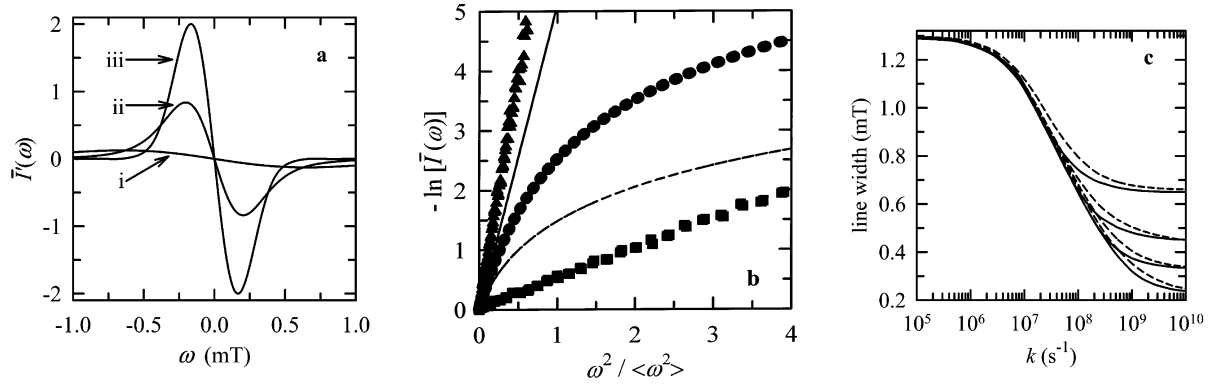

Figure 3. Characteristics of oligomer EPR spectra narrowed by spin motion. In all cases, motion was considered to occur with identical rates (k) between nearest neighbors only. Panel a shows first-derivative curves computed from digitally filtered absorption-mode spectra for (i) the slow-motion limit where the rate $k \ll 10^6$ s^{-1}, (ii) the intermediate-motion regime where $k \approx 6 \times 10^8$ s^{-1}, and (iii) the fast-motion limit where $k \gg 10^9$ s^{-1}. The data were calculated for a closed-loop 16-mer with a width ($\Delta\omega_M$) of the unperturbed basic unit spectral distribution of 1.3 mT. The spectral widths are obtained from the differences of the magnetic field loci of the extrema of the curves. Panel b displays graphs of $-\ln[\bar{I}(\omega)]$ versus $\omega^2/\langle\omega^2\rangle$ that were calculated from absorption-mode spectra corresponding to the curves shown in panel a. Here ω is the magnetic field and Δ_M^2 is the second moment of the unperturbed basic unit spectral distribution. The symbols denote curves calculated from the closed-loop 16-mer absorption-mode spectra, and the solid and dashed lines represent curves calculated from Gaussian and Lorentzian absorption-mode shapes, respectively, the widths of which were identical to that of the $k \approx 6 \times 10^8$ s^{-1} spectrum. In this logarithmic form, a Gaussian shape will exhibit a linear variation with $\omega^2/\langle\omega^2\rangle$. The linearity of the slow- (■) and fast- (▲) modulation limit curves demonstrates that the corresponding spectra are Gaussian. The intermediate (●) modulation spectrum clearly deviates from a Gaussian line shape. It is additionally discerned that the curve lies between those calculated for the Gaussian and Lorentzian functions. Such line shapes are found to be characteristic of the intermediate regime of motion. Similar shape and width variations are also detected for open-chain N-mer spectra. Panel c displays width versus rate profiles of closed-loop (—) and open-chain (− −) N-mers. The curves (top to bottom in the fast-motion regime) were calculated with $N = 4$, 8, 16, and 32 with a $\Delta\omega_M$ of 1.3 mT. For all N, line widths of about 1.3 mT are recovered when the rate is less than about 10^6 s^{-1}. The widths decrease precipitously with increasing rate in the 10^6-10^9 s^{-1} region and then slowly converge to limiting values with increases in the rate beyond 10^9 s^{-1}. The fast-motion limit width values in all cases are reduced relative to $\Delta\omega_M$ by factors of $\sqrt{N}$, as expected on the basis of the Norris−Katz delocalization or fast-motion limit model.[37] It is discerned that significant segments of the width versus rate profiles calculated for different N coincide in the intermediate regime. The line shapes in these segments are found to be essentially indistinguishable as well. We note that the fast-motion limit is reached more rapidly for closed-loop oligomers than for open-chain systems of the same lengths. This effect occurs because of the greater connectivity of the closed-loop oligomers where a given rate results in more efficient averaging of the magnetic environments relative to the corresponding open-chain systems. It is evident that the phenomenon should become progressively less pronounced with increasing N. Visual inspection of the data indeed reveals this to be the case.

T_g to λ_s at high temperatures where $T \gg T_g$. The standard electron-transfer description of Hopfield is recovered when the glassing function $f(T)$ is set to unity at all temperatures.

Later in this article, we discuss the reasons that inter-B880 charge migration can be nominally considered to be an isoenergetic process. On this basis, we will interpret the temperature dependence of the inter-B880 transport rates using Hopfield's model, which is obtained from eq 4 as described above, and Tang's model, which is outlined next, and compare the results to those obtained on the basis of Hoffman and Ratner's approach (eq 4). Tang's multimode description is obtained from a spin-boson model-based expression for the electron-transfer rate using a steepest descent method.[18] Assuming a nonadiabatic process, the rate for an isoenergetic electron-transfer reaction was derived as

$$k = \frac{4\pi^2}{h} \frac{V^2}{\sqrt{2\pi \sum_j h^2 \nu_j^2 \gamma_j^2 \operatorname{csch}(h\nu_j/2k_BT)}} \times \exp[-\sum_j \gamma_j^2 \tanh(h\nu_j/4k_BT)]$$

$$\lambda \approx \sum_j \lambda_j \approx \sum_j h\nu_j \gamma_j^2 \qquad (5)$$

where V is the electronic coupling matrix element, ν_j represents the frequencies of the vibrational modes coupled with strengths γ_j to the electron-transfer reaction, and λ is the total reorganization energy, which is given as the sum of the reorganization-energy contributions of the various vibrational modes coupled to electron transfer.

III. Analysis, Results, and Discussion

We consider inter-B880 charge transport to occur as a stochastic process between a specific set of well-defined basic units. The basic unit, which engenders the unperturbed B880$^{\bullet+}$ spectral distribution, consists of one or more BChl*a*s over which the unpaired electron is strongly delocalized. Thermally activated hole/electron transport between the basic units causes random fluctuations of the electron−nuclear hyperfine interactions, and this produces temperature-dependent changes in the B880$^{\bullet+}$ spectral shape and width. In this work, we attempt to infer details regarding the underlying charge-transfer process through simulations of the observed EPR line narrowing. To conduct an effective analysis of inter-B880 charge transport on the basis of the EPR model, it is essential to place bounds on the parameter values used for the inhomogeneous width of the unperturbed B880$^{\bullet+}$ spectrum and the number of sites or basic units. It is also critical to use an appropriate model for the connectivity of the B880s in the oligomers. We first address these concerns in sections A−C on the basis of our B880$^{\bullet+}$ EPR data, the known EPR characteristics of BChl*a*$^{\bullet+}$ species, and available structural information for LH1. Results of the charge-transport analysis are reported and discussed in sections D and E.

A. Width of the Unperturbed B880$^{\bullet+}$ Spectrum. It is clear that the inhomogeneous width ($\Delta\omega_M$) of the unperturbed spectral distribution must be determined when charge transport is significantly slowed or halted so that the spectrum is in the slow-

motion limit (Figure 3c). This condition is established to a good approximation at 6 K, where a Gaussian B880$^{\bullet+}$ spectrum with a 1.3-mT width is detected. Some ambiguity in this value arises, however, because in addition to charge transport, which is the dominant process, the dynamics of methyl group rotations may contribute to a small extent to the temperature dependence of the B880$^{\bullet+}$ spectral width. This is based on investigations of monomeric BChl*a*$^{\bullet+}$ in methanol−glycerol glass that show that the width is increased from 1.35 mT at 80 K to 1.4 mT at 6 K because of the freezing of the rotations of methyl groups located on rings I and III of the macrocycle.[26] Analogous small changes are also observed for the radical cation of the primary electron donor of reaction centers, P865$^{\bullet+}$, which is a strongly coupled dimer of BChl*a*s (Figure 2). It is not possible in our studies to decouple the effect of charge transport from that due to methyl group rotations. Hence, to allow for contingencies, we have conducted simulations with values of $\Delta\omega_M$ ranging from 1.25 to 1.4 mT. The lower limit accounts for the possibility that the observed $\Delta\omega_M$ of 1.3 mT is due to frozen rotations (and transport) and that at higher temperatures (nominally >80 K) rapid rotations lead to a decrease in $\Delta\omega_M$ by 0.5 mT. The upper limit accounts for the situation where the actual $\Delta\omega_M$ is 1.4 mT and methyl group rotations are completely hindered at all temperatures so that $\Delta\omega_M$ is unaltered. In this case, the slightly reduced 6 K width is ascribed to residual slow charge transport.

B. Number of Sites in the B880 Oligomer. The number of sites or basic units in the B880 oligomer must be deduced from structural information available for LH1, where the desired quantity is the number of BChl*a*s per oligomer, and data from experiments that interrogate the number of strongly coupled BChl*a*s in the basic unit, B880$^{\bullet+}$. The ratio of the total number of BChl*a*s in the oligomer to the number of BChl*a*s in a basic unit is the number of sites (N) over which charge migration occurs.

In principle, the supermolecular nature of B880$^{\bullet+}$ can be deduced from $\Delta\omega_M$, where generally a smaller value relative to that of monomeric BChl*a*$^{\bullet+}$ indicates delocalization of the unpaired electron over more than one macrocycle.[16] The 1.3-mT $\Delta\omega_M$ detected for B880$^{\bullet+}$ at 6 K lies between 1.4 and 0.99 mT, which are the experimentally observed and expected values, respectively, for in vitro monomeric BChl*a*$^{\bullet+}$ and symmetric delocalized (BChl*a*)$_2^{\bullet+}$ at that temperature. The observed $\Delta\omega_M$, given the repeating $\alpha\beta$ structure of LH1, indicates that B880$^{\bullet+}$ corresponds to either BChl*a*$^{\bullet+}$ or a highly asymmetric delocalized (BChl*a*)$_2^{\bullet+}$ species wherein the spin densities are very unequally distributed over the two components. The slightly reduced width in the case of a monomer can arise from slow residual transport between monomeric BChl*a*s. In the case of an asymmetric dimer, the uneven spin-density distribution can arise from deviations from C_2 symmetry, where the deviations can be caused by dissimilar protein environments surrounding the macrocycles and/or perturbations of the BChl*a* structures.[16] The above data in conjunction with structural information for LH1 from electron microscopy studies,[7,9] which indicate 16 $\alpha\beta$ units or 32 BChl*a*s per LH1, specify N as either 16 dimers or 32 monomers. (The number of BChl*a*s deduced through biochemical assays generally ranges from 24 to 32 pigments per LH1 complex.[7,27] The results of biochemical assays and electron microscopy studies when taken together suggest that a circular oligomer with 16 $\alpha\beta$(BChla_2) units is the most probable structure.) Inasmuch as the analysis is concerned, the uncertainty regarding N is primarily an irritant to aesthetic sensibilities because spectra calculated with $N = 16$ and 32 (or even $N =$ 12, 16, 24, 32) are essentially indistinguishable in the intermediate motion regime (Figure 3c), which is the regime indicated by the experimental spectral characteristics in the investigated temperature range.

We note that whereas it is not possible to establish the delocalized nature of B880$^{\bullet+}$ conclusively on the basis of X-band EPR data, evidence from other experiments suggests that it may be best considered as a dimer. Electrochemical and chemical redox titrations of the LH1 BChl*a*s yield midpoint potentials (E_m) between about 0.55 and 0.6 V, which are reduced compared to the 0.66 V value detected for pentacoordinated monomeric BChl*a* in protic solvents.[19,20,28] A decreased value of about 0.5 V is also observed for the primary donor, P865, of reaction centers. The reduced E_m of P865, and by analogy that of B880, has been attributed to strong inter-BChl*a* interactions. It is found that B880$^{\bullet+}$ and P865$^{\bullet+}$ exhibit near-infrared (NIR) absorption bands at about 1230 and 1250 nm, respectively, but such a band is not detected for monomeric BChl*a*$^{\bullet+}$.[19,20] The P865$^{\bullet+}$ NIR band has been attributed to a triplet-coupled Q_y absorption.[29] Calculations indicate that the band intensity is derived from the strength of intermolecular interactions such that the transition becomes asymptotically forbidden at large separations. However, it is not immediately clear what the coupling strength needs to be to produce the observed intensity in the case of B880$^{\bullet+}$. Finally, the optical and electrooptical characteristics of B880 are extremely similar to those of P865.[30] The aforementioned information, in conjunction with the 6 K EPR data, suggests that B880$^{\bullet+}$ may be best represented as an asymmetric dimer. Hence, it must be considered that transport between $N = 16$ asymmetric dimers is the more probable description of charge migration in B880 oligomers.

C. Connectivity in the B880 Oligomer. The analysis of inter-B880 charge transport is critically contingent upon assumptions regarding the migration pathway(s) of the holes in the oligomers. In this study, only intraoligomer transport between nearest-neighbor B880s was considered. The nonnearest neighbor and interoligomer pathways were neglected because the larger separations lead to much smaller electronic couplings, which in turn lead to vastly diminished rates between the more distant molecules compared to nearest neighbors. To elaborate further, structural data for LH1 indicate that the B880s are arranged as an overlapping array sandwiched between inner and outer walls formed by the α and β peptides.[7,9,12] This suggests that the B880s within an oligomer are well insulated from the surroundings and macrocycles on neighboring complexes. Inasmuch as interoligomer pigment distances are concerned, modeling studies on antenna complexes yield separations of about 2.2 nm between BChl*a*s on neighboring LH1 and LH2 complexes.[12] Similar separations should be obtained for neighboring LH1 complexes. With regard to intraoligomer distances, crude estimates obtained from the computationally modeled structure of LH1 indicate nearest-neighbor and next-nearest-neighbor dimer separations of about 0.4−0.5 nm and 1.8−2.0 nm, respectively.[12] Given that the electron-transfer rate decreases with increasing distance as $k \propto \exp[-\beta(R - R_0)]$, where β ($\beta \approx 10$ nm^{-1}) is an attenuation coefficient, R is the distance between the molecules, and R_0 ($R_0 \approx 0.36$ nm) is the separation at van der Waals contact,[1] it is calculated using the distances that the intraoligomer next-nearest-neighbor and interoligomer rates are 6 to 7 orders of magnitude smaller than the nearest-neighbor rate so that the former processes can be neglected. Similar conclusions are drawn if transport is assumed to proceed between monomeric BChl*a* basic units.

Another issue pertaining to the connectivity of B880s is whether the oligomers form closed-loop rings. As noted earlier,

electron micrographs of LH1 complexes in many instances show circular structures.[7−10] Most relevant to our study is the observation of rings for LH1 complexes isolated from *Rb. sphaeroides*, where the dimensions are sufficient to encompass 16 $\alpha\beta$ units.[9] Exceptions to closed-loop structures may occur. This is suggested by an investigation of membranes containing LH1 and reaction centers (RCs), where electron micrographs show $\alpha\beta$ units forming C-shaped open-chain structures that partially encircle RCs.[11] The issue of closed-loop versus open-chain oligomers is, however, not very critical to the analysis because for a given N, particularly the larger N, and $\Delta\omega_M$, the calculated width versus rate profiles and spectral shapes for the two structures do not deviate significantly from one another (Figure 3c). In this study, we have modeled the B880 oligomer only as a closed-loop system but note that extremely similar results are to be expected on the basis of an open-chain model.

D. Description of Charge Transport as an Isoenergetic Process. The LH1 BChl*a*s are held in the hydrophobic α-helical segments of the α and β peptides by histidine residues that bind to the central Mg atom of the macrocycles.[6] Because the pigments are situated in similar environments—nominally identical environments if $B880^{\bullet+}$ is a dimer and extremely similar environments if $B880^{\bullet+}$ is a monomer—the free-energy gap for the charge-migration process must be to a good approximation equal to zero. This viewpoint is supported by results of room-temperature chemical and electrochemical redox titrations of the B880s, where the data show evidence of only a single type of redox-active B880 species.[19,20,28] In this section, we report on the analysis of inter-B880 charge transport based on the above considerations. The process is assumed to be isoenergetic, and heterogeneity is neglected. In particular, medium relaxation effects, which would generate traps in the oligomers, are disregarded. For simplicity, we have also assumed equal electronic couplings between the basic units.

Per the discussion of sections A−C, simulations were conducted with $\Delta\omega_M = 1.25$, 1.3, 1.35, and 1.4 mT and $N =$ 16 and 32 for intraoligomer nearest-neighbor transport along a closed loop. The considerations for inter-B880 charge migration elucidated in the previous paragraph and the assumptions regarding the connectivity of the B880s result in a cyclic tridiagonal form for matrix **W**, where all nonzero off-diagonal elements are equal to the charge-transport rate (k) and all diagonal elements are equal to $(-T_2^{-1} - 2k)$. The assumptions regarding transport also result in identical equilibrium occupational probabilities at all sites so that the elements of $\boldsymbol{\varphi}$ become equal to $(1/N)$. Spectral simulations were conducted as described in section II. A. The charge-transport rate at a given temperature was determined by varying this parameter until good visual agreement was detected between the simulated and experimental spectra. A more convenient alternative procedure was also attempted where the rates were extracted by interpolating the experimental widths into calculated width versus rate profiles. The rates determined by the two procedures, when checked at a few temperatures, showed good agreement.

We attempted to describe the temperature profiles of the rates, displayed in Figure 4a, with Hopfield's two-mode model (section II. B: eq 4 with $f(T) = 1$ for all T).[17] It was not possible to obtain a satisfactory fit to any of the profiles despite the fact that all five parameters (V, $\nu_{(o)}$, λ_o, $\nu_{(i)}$, λ_i) were varied in the fitting procedure. The failure occurs because the rapid rate variation at about 245 K cannot be captured by Hopfield's model. This rate variation of course mirrors the rapid width change at this temperature (Figure 2). Reasonable descriptions of the profiles could be obtained in the 6−245 K temperature

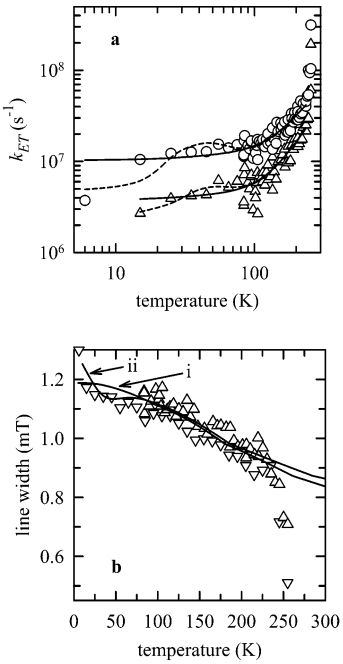

Figure 4. Panel a displays inter-B880 charge-transport rate versus temperature profiles extracted from experimental data and fits to the extracted rate profiles with Hopfield's and Tang's models for nonadiabatic electron transfer.[17,18] The rates were obtained by interpolating the experimental widths into calculated width versus rate profiles. The assumptions for transport and the EPR model were that migration occurs via a nearest-neighbor mechanism along a closed loop containing 16 dimeric basic units. The nearest-neighbor rates were taken to be identical so that the process corresponds to isoenergetic transport between equally coupled basic units. The rates that are shown were extracted from profiles calculated with basic unit widths, $\Delta\omega_M$, of 1.25 (△) and 1.4 mT (○); the rates extracted from profiles calculated with $\Delta\omega_M$ values of 1.3 and 1.35 mT lie between these data and are not displayed here to avoid clutter. Extremely similar profiles are obtained when migration is considered to occur along a closed loop containing 32 monomeric basic units (data not shown). The solid and dashed lines respectively represent fits to the profiles in the 6−245 K temperature range with Hopfield's and Tang's models for nonadiabatic electron transfer.[17,18] It was not possible to describe the full temperature variation of the inter-B880 rates with either electron-transfer model. Panel b shows comparisons of calculated width versus temperature profiles (lines) to experimental $B880^{\bullet+}$ data, where the experimental data are for $B880^{\bullet+}$ elicited with (△) 7 and (▽) 8 μM final concentrations of potassium ferricyanide.[4] The assumptions for inter-B880 charge transport were as outlined above. The calculated profiles were obtained with (i) Hopfield's model and (ii) Tang's model. In both cases, a $\Delta\omega_M$ of 1.3 mT was used. We discern that the profile calculated with Tang's model better describes the low-temperature ($T < 50$ K) region. Line width versus temperature data calculated using either Hopfield's model or Tang's model fail to capture the precipitous line-width change that is experimentally detected for $B880^{\bullet+}$ at about 245 K.

range with the following set of parameters: $V = 1$ cm^{-1}, $\nu_{(o)} = 3 \times 10^{-6}$ cm^{-1} (fits are not very sensitive to this parameter but a small value is always recovered), $\lambda_o = 204-225$ cm^{-1}, $\nu_{(i)} = 75-83$ cm^{-1}, $\lambda_i = 1331-1128$ cm^{-1}. The total reorganization energy is about 1535−1353 cm^{-1}. To determine whether the results were model-dependent, we fit the profiles in the 6−245 K temperature range with Tang's expression for nonadiabatic electron transfer (section II. B: eq 5) using two vibrational modes.[18] We note that this model better describes the low-temperature region (Figure 4). The fits yielded $V =$ 1.2−1.1 cm^{-1}, $\nu_o = 54-32$ cm^{-1}, $\lambda_o = 196-143$ cm^{-1}, $\nu_i =$ 438−421 cm^{-1}, and $\lambda_i = 2421-1994$ cm^{-1}. The vibrational frequencies and corresponding reorganization energies are designated as outer sphere (ν_o, λ_o) or inner sphere (ν_i, λ_i) on

the basis of the extracted values of the frequencies. The total reorganization energy is 2617−2136 cm^{-1}. Except for the matrix element, the parameter values obtained from the two different models are not in good agreement. However, we have discerned that both models yield λ_o values that are smaller than the λ_i values, and the total reorganization energies are within a factor of 2. We also attempted to describe the full temperature dependence with Tang's expression using more than two vibrational modes.

These efforts failed. Figure 4b compares calculated line width versus temperature profiles to experimental data. The simulations were conducted with electron-transfer parameters in the ranges reported above and with a $\Delta\omega_M$ of 1.3 mT. The behavior of the calculated line-width data mirrors the variations exhibited by the fits to the rate versus temperature profiles, as expected. It is found in general that profiles calculated using Tang's model better match the experimental data in the low-temperature ($T < 50$ K) region. Line-width profiles calculated with either Hopfield's model or Tang's model fail to capture the rapid width variation detected for $B880^{\bullet+}$ at 245 K.

E. Description of Charge Transport with Temperature-Dependent Energetics. Rapid decreases of the electron-transfer rate in the 250−200 K range upon cooling have been observed for reactions in protein systems such as mixed-metal hemoglobin hybrids (Fe^{2+}(CN)porphyrin → (Mg)porphyrin$^+$, Fe^{2+}(1-MeIm)-porphyrin → (Zn)porphyrin$^+$),[3] oxidized B820 complexes (BChl*a*$^{\bullet+}$ ⇌ BChl*a*),[15] and photosynthetic reaction centers ($quinone_B^{\bullet-}$ → $P865^{\bullet+}$).[5] The decrease in rates is attributed to temperature-dependent changes of the energetics caused by the progressive slowing down of solvent motion. According to this view, the damping of low-frequency motion upon lowering the temperature restricts the contribution of the full reorganization energy and alters the free-energy gap for the process by precluding complete relaxation of the medium around the products. The consequences are expected to be particularly pronounced at temperatures below the glassing temperature of the medium. In this section, we report on the analysis of inter-B880 charge transport on the basis of Hoffman and Ratner's description for electron transfer in glassy media (section II. B).[2] We adopt this interpretation on the basis of the precedents and because it was not possible to describe inter-B880 charge transport successfully as an isoenergetic process, which it is nominally.

For simplicity, we have again assumed identical electronic couplings between the basic units, that is, the consequences of structural disorder are neglected. Additionally, we assume that the electronic couplings are independent of temperature. In the context of electron transfer through a protein medium, temperature-dependent electronic couplings can occur, for instance, because of dielectric fluctuations of the medium.[31] In the case of the B880 oligomers, a different situation arises. The LH1 B880s are held by the α and β peptides, where by analogy to LH2 complexes[13,14] it is expected that no intervening protein medium exists between the pigments. The B880s are thought to form an overlapping circular array similar to the B850 ring of LH2 complexes.[12] Under this circumstance, any significant temperature-dependent displacements that modulate the inter-B880 separations will produce strong variations of the electronic couplings. It is thus possible that the strong turn on of the rates is due to changes in the inter-B880 electronic couplings induced by the unfreezing of modes at temperatures greater than the glass-transition temperature. In our experimental work, we also observed progressively increasing sample dielectric absorption at temperatures greater than about 240 K. (The sample remains frozen at least until 265 K, as determined by visual inspection.) This indicates that motions in the gigahertz frequency range are activated at these temperatures. An interesting possibility is that these motions are coupled to the inter-B880 charge-transport process so that activation of the gigahertz frequency modes results in increased rates. If this is so, then another situation must be considered wherein electron tunneling occurs on or close to the time scales of these gigahertz (nanosecond) motions, in which case the process can no longer be treated within the framework of the Condon approximation.[32] In this analysis, we neglect the above possible complications and consider only the energetic consequences of the activation/freezing of low-frequency motions on the rates of inter-B880 charge transport.

According to Hoffman and Ratner's model, the slow dynamics of medium relaxation results in a temperature-dependent free-energy gap: $\Delta G(T) = \Delta G^0 + \lambda_o[1 - f(T)]$. We take ΔG^0 (the equilibrium free-energy gap) to be equal to zero on the basis of the considerations outlined in the previous section. Inter-B880 charge transport can then be modeled as a nonisoenergetic process with $\Delta G(T) = \lambda_o[1 - f(T)]$. At low temperatures such that $T < T_g$, low-frequency motions are (assumed to be) completely quenched. This situation is described by setting $f(T) = 0$ so that $\lambda(T) = \lambda_i$ and $\Delta G(T) = \lambda_o$. As the temperature increases past T_g, the low-frequency modes become activated, which is characterized by an exponentially increasing contribution of $\lambda(T)$, specifically $\lambda_o(T)$, and decreasing $\Delta G(T)$. Finally, complete unglassing occurs when $T \gg T_g$. This circumstance is described by $f(T) \rightarrow 1$ so that $\lambda(T) \rightarrow \lambda_s$ and $\Delta G(T) \rightarrow 0$. For simplicity, we have adopted a model where alternate sites are considered to be traps. The rate into the traps (k_{in}) is calculated with eq 4, in which $[\Delta G^0 + \lambda_s]$ is replaced with $[-\Delta G(T) + \lambda(T)] = \{-\lambda_o[1 - f(T)] + \lambda(T)\}$. The rate out of the traps is then calculated as $k_{out} = k_{in} \exp[-\Delta G(T)/k_BT] = k_{in} \exp[-\lambda_o[1 - f(T)]/k_BT]$. It seems reasonable to connect k_{in} and k_{out} by the equilibrium-type relation because Hoffman and Ratner's premise is that $\Delta G(T)$ describes on average the free-energy gap between products formed in nonequilibrium states and the reactant states.

Calculations were conducted with $\Delta\omega_M = 1.25$, 1.3, 1.35, and 1.4 mT and $N = 16$ and 32 for intraoligomer nearest-neighbor transport along a closed loop. The considerations for inter-B880 charge migration elucidated in the previous paragraph and the assumptions regarding the connectivity of the B880s result in a cyclic tridiagonal form for the matrix **W**. The nonzero elements of **W** are given by the following algorithm. For odd i, $w_{ii+1} = k_{in}$, $w_{i+1i} = k_{out}$, and $w_{ii} = (-T_2^{-1} - 2k_{out})$, and for even i, $w_{ii+1} = k_{out}$, $w_{i+1i} = k_{in}$, $w_{ii} = (-T_2^{-1} - 2k_{in})$; $w_{1N} = k_{in}$ and $w_{N1} = k_{out}$. The assumptions regarding transport result in occupational probabilities that are given as $\varphi_i = 2k_{in}/N(k_{in} + k_{out})$ for odd i and $\varphi_i = 2k_{out}/N(k_{in} + k_{out})$ for even i. The EPR line-narrowing simulations were conducted as described in section II. A. The parameters governing the charge-transport process were extracted by varying the values until reasonable agreement was detected between calculated width versus temperature profiles and the experimental data.

The description of inter-B880 transport on the basis of Hoffman and Ratner's rate expression (eq 4) involves seven parameters, several of which can be fixed at reasonable values. To begin with, the pseudoactivation energy (B) and glass-transition temperature (T_g), which appear in the unglassing function $f(T)$, were fixed at 100 and 225 K, respectively. These values were chosen so as to capture the rapid decrease of the line width (increase of k_{in} and k_{out}) with increasing temperature starting at about 245 K. The values correspond closely to those

employed by Dick et al. to describe electron transfer in mixed-metal hemoglobin hybrids[3] and by us to describe charge transport in oxidized B820 complexes.[15] We find that the values of B and T_g can be altered within reasonable bounds without seriously impacting any of the other parameters. Thus, an equivalent description can be obtained with $B = 150$ K and $T_g = 200$ K. Next, the low-frequency vibration ($\nu_{(o)}$) was fixed at a value of about 14 cm^{-1} ($T_c^{(o)} = 20$ K), which is identical to the value used in previous studies. The outer-sphere reorganization energy (λ_o) was fixed at 125 cm^{-1} on the basis of our earlier work on inter-BChl*a* charge transfer in oxidized B820 complexes.[15] Later in this section, we will discuss reasons that λ_o cannot be large. We assumed that the values obtained from the analysis reported in the previous section for the electronic coupling matrix element (V) were in fact reasonable estimates of this parameter. Accordingly, V was fixed at about 1 cm^{-1}. Thus, the only adjustable parameters were the high-frequency vibration ($\nu_{(i)}$) and the associated innersphere reorganization energy (λ_i).

Width versus temperature profiles calculated with $\nu_{(i)} = 70$ cm^{-1} and $\lambda_i = 6-8$ cm^{-1} capture quite accurately the main characteristics of the experimental data (Figure 5). To reiterate, the charge-transport parameter set consists of $V \approx 1$ cm^{-1}, $\nu_{(o)} \approx 14$ cm^{-1}, $\lambda_o = 125$ cm^{-1}, $\nu_{(i)} = 70$ cm^{-1}, $\lambda_i = 6-8$ cm^{-1}, $B = 100$ K, and $T_g = 225$ K. The 1-cm^{-1} value of the electronic coupling matrix element, V, satisfies fairly well the condition $V \ll k_B T$, which indicates that it is reasonable to consider inter-B880 transport to be a nonadiabatic process.[33] The value for the high-frequency vibrational mode, $\nu_{(i)}$, of 70 cm^{-1} is small compared to typical numbers for high-frequency vibrations. (For example, the C−H and C═C stretching frequencies are on the order of 3000 and 1600 cm^{-1}, respectively.) Within the framework of the electron-transfer model, the small $\nu_{(i)}$ value is consistent with a situation wherein the low-frequency motions are not completely quenched below T_g. In this picture, low-frequency motions represented by the 70-cm^{-1} mode that persist below T_g are responsible for transport down to liquid He temperatures. It is not unusual that genuine high-frequency modes are not strongly coupled to inter-B880 transport. In a large delocalized π system such as BChl*a*, the formation of a hole is not expected to result in large bond-length changes.

We discern that the calculated curves deviate from the experimental data in the low-temperature ($T < 50$ K) region. This may reflect contributions to the shape of the experimental width versus temperature profiles from activated methyl group rotations. In particular, the very rapid B880$^{\bullet+}$ width decrease detected in the 6−20 K region is reminiscent of that observed for P865$^{\bullet+}$ (Figure 2). In our calculations, we have used fixed values for $\Delta\omega_M$ and have neither scaled this parameter with temperature nor included a dynamic picture of the rotations in the EPR model to account for line narrowing/broadening due to methyl group rotations in greater detail. Another possible reason for the deviation pertains to the electron-transfer model itself. We find that Tang's model captures the curvature in the low-temperature region whereas Hopfield's model does not (Figure 4b). (With respect to Tang's model, factors containing $v_{(o)}$ give rise to this low-temperature feature.)

The temperature profiles of k_{in} and k_{out} calculated with the electron-transfer parameter set reported earlier are displayed in Figure 6a. These rates are to be considered as some averaged representation of the heterogeneous rate distribution characterizing the inter-B880 transport process. In the case of k_{in}, a temperature-independent region is detected in the 6−60 K range whereas k_{out} shows a strong increase with temperature in the same range. The temperature independence of k_{in} is characteristic of nuclear tunneling, which in this case is enhanced because the reaction occurs in the inverted region ($|-\Delta G(T)| \gg \lambda_i$, Figure 6b). In the same range, k_{out} exhibits activated behavior because this process occurs deep in the normal region. The rates increase sharply at temperatures greater than 225 K ($T_g = 225$ K). These increases are a consequence of the exponentially increasing contribution of λ_o and decreasing $\Delta G(T)$. Figure 6b displays the temperature dependences of $\Delta G(T)$ and $\lambda(T)$. We note that the full contribution of λ_o ($\lambda_o = 125$ cm^{-1}) is not available at 255 K, which is the highest temperature at which experimental data is collected. An extrapolation of $\lambda(T)$ to higher temperatures shows that the full contribution is unavailable even at room temperature. This circumstance is similar to that found by Dick et al. for electron transfer in mixed-metal hemoglobin hybrids.[3] The temperature dependences in these investigations were also analyzed with eq 4. The researchers suggest that the protein functions as the primary solvent for the redox cofactors and propose that even at room temperature the protein behaves like a frozen glass with respect to the low-frequency motions coupled

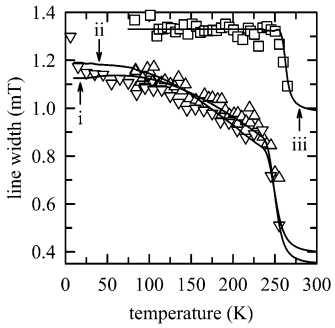

Figure 5. Comparison of calculated width versus temperature profiles (lines) to the experimental data of B880$^{\bullet+}$ (△, ▽) and B820$^{\bullet+}$ (□). The B880$^{\bullet+}$ samples were generated with (△) 7 and (▽) 8 μM final concentrations of potassium ferricyanide,[4] and the B820$^{\bullet+}$ sample was generated with a 100 μM final concentration of potassium ferricyanide.[15] In the case of B880$^{\bullet+}$, the assumptions for transport and the EPR model were that migration occurs via a nearest-neighbor mechanism along a closed loop containing 16 dimeric basic units. Alternate sites along the oligomer were considered to be traps with temperature-dependent depths. The rates into and out of the traps were calculated with Hoffman and Ratner's model for electron transfer.[2] The simulated curves shown for B880$^{\bullet+}$ are for basic unit widths ($\Delta\omega_M$) of (i) 1.25 and (ii) 1.4 mT. Profiles calculated with $\Delta\omega_M$ values of 1.3 and 1.35 mT lie between curves i and ii and are not shown to avoid clutter. Profiles similar to i and ii are also calculated with $\Delta\omega_M$ in the 1.25−1.4 mT range and $N = 32$, where the basic unit is considered to be a monomer, with the same electron-transfer parameters (data not shown). The electron-transfer parameters corresponding to the displayed calculated profiles are $V \approx 1$ cm^{-1}, $\nu_{(o)} \approx 14$ cm^{-1}, $\lambda_o = 125$ cm^{-1}, $\nu_{(i)} = 70$ cm^{-1}, and $\lambda_i = 6-8$ cm^{-1}. In the case of B820$^{\bullet+}$, displayed curve iii was calculated with a $\Delta\omega_M$ of 1.33 mT, and the rate into and out of the trap was calculated with Hoffman and Ratner's model.[15] The electron-transfer parameters are $V = 0.25$ cm^{-1}, $\nu_{(o)} \approx 14$ cm^{-1}, and $\lambda_o = 125$ cm^{-1}. The B820 subunit has elicited much interest because of its possible role as a structural and functional building block of B880 oligomers (LH1 complexes). With regard to the EPR of the radical cations and charge-transport properties, however, it is seen that B820 does not function as a building block of the B880 oligomers. Charge transport in oxidized B820 subunits is substantially quenched when the temperature is reduced below the glass-transition temperature ($T_g = 200-225$ K) whereas in the case of oxidized B880 oligomers charge transport persists to liquid He temperatures. Within the framework of the electron-transfer model, the difference can be attributed to the 70-cm^{-1} mode, which in the case of B880 oligomers is not frozen below T_g, whereas in the case of B820 subunits the 70-cm^{-1} mode is either frozen below T_g or does not exist.

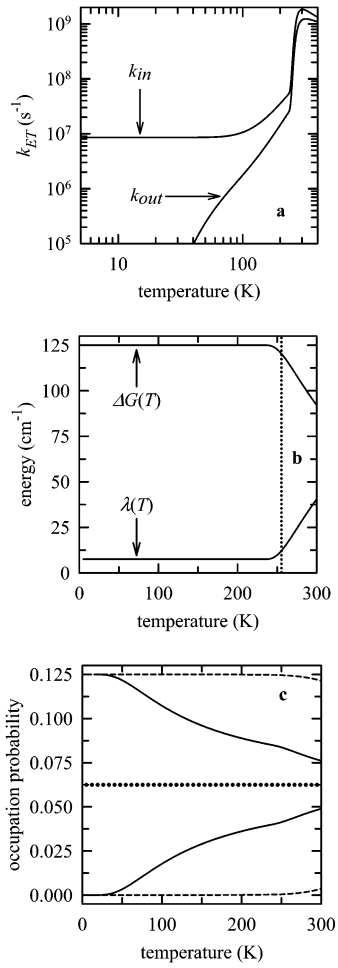

Figure 6. Panel a displays the temperature dependence of the calculated charge-transfer rates into (k_{in}) and out of (k_{out}) traps in the B880 oligomers. The shown rates, which were calculated with Hoffman and Ratner's electron-transfer model,[2] resulted in width versus temperature profiles that well described the experimental data (Figure 5). The electron-transfer parameters used for rate calculations are $V \approx 1$ cm^{-1}, $\nu_{(o)} \approx 14$ cm^{-1}, $\lambda_o = 125$ cm^{-1}, $\nu_{(i)} = 70$ cm^{-1}, $\lambda_i \approx 7$ cm^{-1}, $T_g = 225$ K, and $B = 100$ K. Panel b displays the temperature dependences of the reorganization energy ($\lambda(T) = \lambda_i + \lambda_o(T) = \lambda_i + \lambda_o f(T)$) and the free-energy gap ($\Delta G(T) = \lambda_o[1 - f(T)]$). We discern that $\Delta G(T)$ is greater than $\lambda(T)$ in the investigated temperature range (marked by the vertical dotted line) and even at 300 K. This implies that transport into the traps, which is characterized by an energy gap of $[-\Delta G(T)]$, occurs in the inverted region, and migration out of the traps occurs in the normal regime of electron transfer. It is additionally noted that the full contribution of the outer-sphere reorganization energy, $\lambda_o = 125$ cm^{-1}, is not available at 255 K, which is the highest temperature at which experimental data is collected, or even at room temperature. Panel c shows the temperature dependences of the occupational probabilities of the spins in the two distinct sites of the B880 oligomer. In Hoffman and Ratner's model, $\Delta G(T)$ is related to the outer-sphere reorganization energy (λ_o), and for this reason, the occupational probabilities also become contingent upon λ_o. The curves shown with the solid lines represent occupational probabilities calculated with λ_o set equal to 125 cm^{-1}, and the curves shown with the dashed lines represent data calculated with λ_o set equal to 1000 cm^{-1}. The dotted line in the center is the temperature-independent occupational probability (at each site) that would be expected if the inter-B880 charge-transport process were isoenergetic.

to electron transfer. Our analysis of inter-B880 charge transport on the basis of Hoffman and Ratner's model corroborates these notions.

The conclusion that the LH1 protein functions as the primary solvent for the B880s is consistent with the experimental data, results of the data analysis, and the structural characteristics of the pigment−protein complexes. With regard to the experimental data, the observation of rapid inter-B880 charge transfer in frozen solutions even at cryogenic temperatures indicates that the migration process is for the most part decoupled from bulk water and components in water and is instead controlled by protein vibrations. Our analysis of the data shows that the full reorganization energy is not available at room temperature. This is in accord with the view that the protein functions as the main solvent for the B880s, where the protein matrix retains its glassy characteristics even at room temperature. With respect to structural features, data for LH1 indicate that the B880s are arranged as an overlapping array sandwiched between concentric hydrophobic walls formed by the α and β peptides.[7,9,12] Our conclusion that the protein is the main solvent is consistent with such an architecture. Furthermore, in detergent-isolated samples, the LH1 complexes are located in micelles, and in membrane-bound samples, the proteins are embedded in the lipid bilayer. In either environment, a barrier is present, in addition to the peptide walls, between the B880s and bulk water and ions in the medium. The aforementioned structural features evidently function synergistically so as to decouple inter-B880 charge transport substantially from medium polarization fluctuations and ionic motions. As mentioned earlier, the results of our analysis of inter-B880 charge transport are in accord with the conclusions that Dick et al. draw from their investigations of electron transfer in mixed-metal hemoglobin hybrids.[3] Our interpretation is also in agreement with the results of the electron tunneling studies that Crane and co-workers have conducted on aqueous solutions and single crystals of sensitizer-tagged azurins.[34] The researchers found that the tunneling rates, reorganization energies, and driving forces of the reactions in solution corresponded closely to those observed in single crystals, wherein the lattices contained only 40% water and one-third of the solvent-accessible surface of the tagged azurins was lost. They concluded that bulk water was only minimally involved in azurin electron-transfer reactions. The major contribution to λ_o was assigned to small and distributed conformational changes of the folded polypeptide, and a minor contribution to λ_o was attributed to motions of ordered water of hydration.

The total equilibrium outer-sphere reorganization energy ($\lambda_o = 125$ cm^{-1}) determined for charge migration in B880 oligomers is small compared to typical values in the range of 5000 cm^{-1} observed for reactions in proteins.[1] A straightforward analysis of inter-B880 transport within the framework of Hoffman and Ratner's model, however, shows that λ_o cannot be large. This is because the free-energy gap ($\Delta G(T) = \lambda_o[1 - f(T)]$) and hence the site occupational probabilities (ϕ_i) depend on λ_o. Thus, if λ_o were taken to be 1000 cm^{-1} then it is found that the charges are essentially trapped even at 300 K (Figure 6c). Under these circumstances, the calculated spectra resemble the unperturbed basic unit spectrum from 6 to 300 K, and the simulations cannot capture the experimental width versus temperature profile. The small value of λ_o indicates minimal displacements of the relevant vibrational modes. The results thus suggest that inter-B880 charge transport is accompanied by only extremely small reorganizations of the protein matrix and associated water molecules.

We conclude this section by recapitulating our findings for inter-B880 charge transport: (a) the LH1 protein functions as the main solvent for the B880s, (b) the protein reorganizes minimally during the course of the inter-B880 electron-transfer reactions, and (c) the protein behaves to a significant extent as a frozen glass even at room temperature. These conclusions are based on an analysis of the $B880^{\bullet+}$ experimental data using

Hoffman and Ratner's description of electron transfer in glassy media[2] and structural considerations for LH1.

IV. Summary

The constituent bacteriochlorophyll *a* pigments (B880) of light-harvesting 1 (LH1) complexes can be selectively oxidized to the corresponding radical cations ($B880^{\bullet+}$) with potassium ferricyanide.[19−21] In a prior investigation, we established that the unpaired electrons so elicited migrate within the arrays of B880s.[4,15] The itinerant nature of the spins is revealed through the temperature-dependent changes of the electron paramagnetic resonance (EPR) line-shape characteristics of $B880^{\bullet+}$. At 6 K, a Gaussian-shaped $B880^{\bullet+}$ spectrum with a 1.3-mT width is detected. These features indicate that at extremely low temperatures charge transport is substantially slowed or halted so that the unpaired electron is localized on one or two BChl*a*s, where the latter situation must be regarded as more probable. At higher temperatures, the spectra exhibit non-Gaussian line shapes and decreased line widths. These characteristics are a consequence of charge migration. The most striking experimental feature is the rapid decrease of the width at temperatures greater than about 245 K, which is engendered by a rapid increase in transport rates.

In this work, we have conducted an analysis of inter-B880 charge migration through simulations of the $B880^{\bullet+}$ EPR line-shape characteristics. The simulations were conducted with the assumption that charge migration occurs as a nonadiabatic process between nearest neighbors along a closed loop. Nominally, charge transport between the B880s is a self-exchange reaction. However, the rapid increase/decrease of the rates at 245 K cannot be captured with standard multimode models for electron transfer when inter-B880 transport is considered to be an isoenergetic process. We find that the temperature dependence can be adequately described when the energetic consequences of slow medium relaxation are considered. In particular, we have interpreted inter-B880 charge migration on the basis of Hoffman and Ratner's model for electron transfer in glassy media.[2] Within this framework, the following physically plausible picture emerges. Below the glass-transition temperature ($T_g = 225$ K), low-frequency motions are frozen, and as a result, the outer-sphere reorganization energy (λ_o) becomes substantially unavailable. An additional consequence of the quenching of low-frequency motions is that traps are formed in the B880 oligomers. The combination of these two factors results in slow rates and consequently broad widths at temperatures below T_g. The low-frequency modes become activated at temperatures greater than T_g, which results in a progressively rapid increase of λ_o and a coupled decrease of the trap depths. The rates therefore increase rapidly, and the width decreases at temperatures greater than T_g. On the basis of Hoffman and Ratner's model, we find that the full contribution of λ_o is not available at room temperature. This observation supports the notion that the protein functions as the main solvent for the redox centers and reinforces the view that the protein behaves for the most part as a frozen glass, even at room temperature, with respect to the low-frequency motions coupled to electron transfer.[3]

Acknowledgment. Support from the U.S. Department of Energy, Office of Basic Energy Sciences, Division of Chemical Sciences contract DE-FG02-96ER14675 is gratefully acknowledged. Work performed in Berlin has been supported by the Deutsche Forschungsgemeinschaft (DFG), Sonderforschungsbereich 498 (Teilprojekt A2).

References and Notes

(1) Moser, C. C.; Keske, J. M.; Warncke, K.; Farid, R. S.; Dutton, P. L. *Nature* **1992**, *355*, 796.
(2) Hoffman, B. M.; Ratner, M. A. *Inorg. Chim. Acta* **1996**, *243*, 233.
(3) Dick, L. A.; Malfant, I.; Kuila, D.; Nebolsky, S.; Nocek, J. M.; Hoffman, B. M.; Ratner, M. A. *J. Am. Chem. Soc.* **1998**, *120*, 11401.
(4) Srivatsan, N.; Weber, S.; Kolbasov, D.; Norris, J. R. *J. Phys. Chem. B* **2003**, *107*, 2127.
(5) Schmid, R.; Labahn, A. *J. Phys. Chem. B* **2000**, *104*, 2928.
(6) Zuber, H.; Brunisholz, R. A. In *Chlorophylls*; Scheer, H., Ed.; CRC Press: Boca Raton, FL, 1991; p 627.
(7) Karrasch, S.; Bullough, P. A.; Ghosh, R. *EMBO J.* **1995**, *14*, 631.
(8) Walz, T.; Ghosh, R. *J. Mol. Biol.* **1997**, *265*, 107.
(9) Walz, T.; Jamieson, S. J.; Bowers, C. M.; Bullough, P. A.; Hunter, C. N. *J. Mol. Biol.* **1998**, *282*, 833.
(10) Stahlberg, H.; Dubochet, J.; Vogel, H.; Ghosh, R. *J. Mol. Biol.* **1998**, *282*, 819.
(11) Jungas, C.; Ranck, J.; Rigaud, J.; Joliot, P.; Verméglio, A. *EMBO J.* **1999**, *18*, 534.
(12) Hu, X.; Schulten, K. *Biophys. J.* **1998**, *75*, 683.
(13) McDermott, G.; Prince, S. M.; Freer, A. A.; Hawthornthwaite-Lawless, A. M.; Papiz, M. Z.; Cogdell, R. J.; Isaacs, N. W. *Nature* **1995**, *374*, 517.
(14) Koepke, J.; Hu, X.; Muenke, C.; Schulten, K.; Michel, H. *Structure* **1996**, *4*, 581.
(15) Srivatsan, N.; Norris, J. R. *J. Phys. Chem. B* **2001**, *105*, 12391.
(16) Lubitz, W. In *Chlorophylls*; Scheer, H., Ed.; CRC Press: Boca Raton, FL, 1991; p 903.
(17) Hopfield, J. J. *Proc. Natl. Acad. Sci. U.S.A.* **1974**, *71*, 3640.
(18) Tang, J. *J. Chem. Phys.* **1993**, *99*, 5828.
(19) Gomez, I.; Sieiro, C.; Ramirez, J. M.; Gomez-Amores, S.; del-Campo, F. F. *FEBS Lett.* **1982**, *144*, 117.
(20) Picorel, R.; Lefebvre, S.; Gingras, G. *Eur. J. Biochem.* **1984**, *142*, 305.
(21) Gingras, G.; Picorel, R. *Proc. Natl. Acad. Sci. U.S.A.* **1990**, *87*, 3405.
(22) Kolbasov, D.; Srivatsan, N.; Ponomarenko, N.; Jäger, M.; Norris, J. R. *J. Phys. Chem. B* **2003**, *107*, 2386.
(23) Anderson, P. W. *J. Phys. Soc. Jpn.* **1954**, *9*, 316.
(24) Kubo, R. *J. Phys. Soc. Jpn.* **1954**, *9*, 935.
(25) Molin, N. Y.; Salikhov, K. M.; Zamaraev, K. I. *Spin Exchange: Principles and Applications in Chemistry and Biology*; Springer-Verlag: Berlin, 1980.
(26) Feher, G.; Hoff, A. J.; Isaacson, R. A.; Ackerson, L. C. *Ann. N. Y. Acad. Sci.* **1975**, *244*, 239.
(27) Francke, C.; Amesz, J. *Photosynth. Res.* **1995**, *46*, 347.
(28) Kropacheva, T. N.; Hoff, A. J. *J. Phys. Chem. B* **2001**, *105*, 5536.
(29) Reimers, J. R.; Hush, N. S. *J. Am. Chem. Soc.* **1995**, *117*, 1302.
(30) Sundström, V.; Pullerits, T.; van Grondelle, R. *J. Phys. Chem. B* **1999**, *103*, 2327.
(31) Knapp, E. W.; Fischer, S. F. *J. Chem. Phys.* **1987**, *87*, 3880.
(32) Beratan, D. N.; Hopfield, J. J. *J. Chem. Phys.* **1984**, *81*, 5753.
(33) Closs, G. L.; Miller, J. R. *Science* **1988**, *240*, 440.
(34) Crane, B. R.; Di Bilio, A. J.; Winkler, J. R.; Gray, H. B. *J. Am. Chem. Soc.* **2001**, *123*, 11623.
(35) Bowman, M. K.; Norris, J. R. *J. Am. Chem. Soc.* **1982**, *104*, 1512.
(36) Norris, J. R.; Katz, J. J. In *The Photosynthetic Bacteria*; Clayton, R. K., Sistrom, W. R., Eds.; Plenum Press: New York, 1978; p 397.
(37) Norris, J. R.; Uphaus, R. A.; Crespi, H. L.; Katz, J. J. *Proc. Natl. Acad. Sci. U.S.A.* **1971**, *68*, 625.
(38) Page, C. C.; Moser, C. C.; Chen, X.; Dutton, L. *Nature* **1999**, *402*, 47.